

Preparation and characterization of Bi₂O₃/XNBR flexible films for attenuating gamma rays

Yi-Chuan Liao¹ · Dui-Gong Xu¹ · Peng-Cheng Zhang²

Received: 25 August 2017 / Revised: 25 November 2017 / Accepted: 26 December 2017 / Published online: 29 May 2018
© Shanghai Institute of Applied Physics, Chinese Academy of Sciences, Chinese Nuclear Society, Science Press China and Springer Nature Singapore Pte Ltd. 2018

Abstract A bismuth oxide (Bi₂O₃)-dispersed carboxylated nitrile butadiene rubber (XNBR) flexible film was prepared as a flexible lead-free material for gamma ray (γ -ray) attenuation. However, obtaining a uniform and stable dispersion of Bi₂O₃ in carboxylated nitrile butadiene rubber latex (XNBRL) is a challenge due to sedimentation induced by the remarkable density differences. Here, this challenge was approached by reducing the Bi₂O₃ particle radius, increasing the viscosity of the latex, and adding a dispersant. The experimental results confirmed that Bi₂O₃ was well dispersed in the XNBRL in the concentration range of 30–70 wt%. The mechanical properties demonstrated that the Bi₂O₃/XNBR flexible films had a good resistance to oil, acid, alkali, and hot air. The linear attenuation coefficients of the Bi₂O₃/XNBR flexible films obtained from the experiments were in good agreement with the calculated values. The attenuation efficiencies of the Bi₂O₃/XNBR flexible films with different thicknesses and Bi₂O₃ contents were investigated for a few different γ -ray energies. These results showed that the Bi₂O₃/XNBR

flexible films have wide application prospects for low-energy γ -ray attenuation.

Keywords Carboxylated nitrile butadiene · Rubber latex · Bi₂O₃ · Gamma ray attenuation · Flexible films

1 Introduction

X-rays and γ -rays have a wide range of applications in military, medical, health, scientific, and agricultural industries [1]. However, these rays are also harmful to human health if they are not shielded properly, especially for the staff who handles nuclear materials or radioactive sources [2, 3]. Traditional material structures, such as metal [4, 5], concrete [6], glass [7], and polymer [8, 9], have been commonly used to attenuate γ -rays and other rays, after the addition of heavy metal elements. However, there are situations that require flexible materials for shielding low-energy γ -rays, such as protective shades, clothing, gloves, and helmets. Therefore, many attempts have been made to such develop flexible materials [10–12]. Chai et al. prepared X-ray-shielding materials using W and Bi₂O₃ with methyl vinyl silicone rubber (VMQ) as the matrix [13]. The VMQ composite was fabricated by a plate-vulcanizing machine using solid rubber. However, there are significant differences between solid rubber and rubber latex, such as the molding method, product properties, and applications. Rubber latex is widely used in our daily lives as a flexible material. Carboxylated nitrile butadiene rubber (XNBR) is a copolymer of butadiene, acrylonitrile, and acrylic or meth-acrylic acid. It can be vulcanized through a variety of methods to achieve an excellent performance [14–16]. Furthermore, XNBRL is a latex that can be prepared in any

This work was supported by the National Natural Science Foundation of China (No. 11405149) and the Military Technology Extension Project (No. JMZF201601).

✉ Yi-Chuan Liao
liaoyichuan@caep.cn

✉ Peng-Cheng Zhang
13981102769@163.com

¹ Institute of Materials, China Academy of Engineering Physics, Jianguo 621907, China

² Science and Technology on Surface Physics and Chemistry Laboratory, Jianguo 621908, China

arbitrary shape, possessing good plasticity, elasticity, and resistance to gamma radiation aging [17].

Lead (Pb) has been commonly used at an early stage [18]. However, materials containing Pb are toxic, making post-treatment a large environmental problem. Thus, there is a tremendous need to develop materials free of Pb for γ -ray shielding. The element Bi ($Z = 83$, $A_r = 209$) is located next to Pb ($Z = 82$, $A_r = 207$) in the periodic table of elements. However, Bi is not suitable due to its low melting point (271 °C). The post-treatment of the flexible attenuation material is usually conducted using a burning method. The flexible matrix mainly degrades into CO_2 and H_2O during the burning at a decomposition temperature higher than 500 °C, and the attenuation material is left behind for collection and storage. Bi_2O_3 (with a melting point of 825 °C) has been used in glass for γ -ray attenuation as it is odorless, non-toxic, inexpensive, abundant, and has stable mechanical and chemical properties [19, 20]. All these characteristics indicate that a $\text{Bi}_2\text{O}_3/\text{XNBR}$ film can be used as a flexible material against low-energy γ -rays radiation.

In the present work, XNBRL and Bi_2O_3 were selected as the matrix material and the attenuation material, respectively. Different concentrations of Bi_2O_3 (30–70 wt%) were dispersed in the XNBRL via physical and chemical methods. The mechanical properties (tensile strength, elongation at break, and shore hardness) and low-energy (20–100 keV) γ -ray attenuation properties of the $\text{Bi}_2\text{O}_3/\text{XNBR}$ flexible films were investigated.

2 Experimental

2.1 Preparation of the Bi_2O_3 dispersion

The purity, density, and median diameter (D_{50}) of the Bi_2O_3 powder (Beijing Xing Rong Yuan Technology Co., Ltd.) used in these experiments were 99.9%, 8.9 g cm^{-3} , and $13.7 \mu\text{m}$, respectively. The Bi_2O_3 powder was pre-treated by ball milling for 12 h at 250 rpm. The Bi_2O_3 dispersion consisted of Bi_2O_3 , distilled water, and the dispersant (Nekal, BX, $\text{C}_{18}\text{H}_{24}\text{SO}_3\text{Na}$) with a mass ratio of 1:0.5:0.003.

2.2 Preparation of the XNBRL mixture

The XNBRL mixture consisted of XNBRL, a compounding agent dispersion, KOH, casein, and polyoxyethylene alkyl ether (Levelling Agent O, Pregelal-O). XNBRL (Nipol LX552, Zeon, Japan) is a type of aqueous latex. The solid content was approximately 44 wt%, and the remaining content of the mixture was distilled water. The mixture viscosity was approximately 30 mPa s and its

density approximately 1.02 g cm^{-3} . All chemicals and reagents were used as received. The compounding agent dispersion of the XNBRL included a vulcanizer (S, sulfur), active agent (ZnO, zinc oxide), accelerator (ZDC, zinc diethyl dithiocarbamate), reinforcing filler (C, carbon black), and BX. The composition of the XNBRL mixture is presented in Table 1. The compounding agent was ball-milled at 250 rpm for 12 h. The mass ratio of the compounding agent and distilled water was 1:1.5. The compounding agent dispersion was slowly added to the latex via stirring. Then, the KOH, the casein, and the Pregelal-O solution were mixed into the latex. KOH was used to adjust the pH of the latex to 9–10 to enhance its chemical stability. The viscosity of the latex was controlled by adjusting the contents of the casein and the Pregelal-O solution.

2.3 Preparation of the $\text{Bi}_2\text{O}_3/\text{XNBR}$ flexible films

The $\text{Bi}_2\text{O}_3/\text{XNBR}$ mixture consisted of the Bi_2O_3 dispersion (30–70 wt%) and the XNBRL mixture. For example, the mass fractions of Bi_2O_3 and XNBRL in a 30 wt% $\text{Bi}_2\text{O}_3/\text{XNBR}$ film are 30 and 70 wt%, respectively, normalized by their dry weight, and so on. The Bi_2O_3 dispersion was added to the XNBRL mixture via stirring. Letting the $\text{Bi}_2\text{O}_3/\text{XNBRL}$ mixture equilibrate for 48 h, the desired latex was subsequently obtained after filtration and de-foaming. The $\text{Bi}_2\text{O}_3/\text{XNBR}$ film was then prepared by dip-molding. The dip plate, or mold, was submerged in the latex mixture for several seconds and raised to allow the film to set. After drying, the film was vulcanized in hot air in an oven (100 °C, 60 min). Afterward, the $\text{Bi}_2\text{O}_3/\text{XNBR}$ flexible film was ready for γ -ray attenuation. The thickness of the film was controlled by the number of dips. After a single dip, the thickness of the film was 0.1–0.3 mm. Thicker films were obtained via multiple dips.

2.4 Property characterizations

A digital viscometer (NDJ-5S, Shanghai Ping Xuan Scientific Instrument Co., Ltd.) was used to measure the viscosity of the latex at room temperature. The D_{50} of the Bi_2O_3 particles was measured by a laser particle size analyzer (Mastersizer 2000) using deionized water as the dispersing agent, with a scanning speed of 1000 times/second. The dispersion state of Bi_2O_3 in the rubber latex was analyzed using a scanning electron microscope (SEM, JSM6390 LV, Japan JEOL) and an energy-dispersive spectrometer (EDS). Fourier transform infrared (FTIR) spectra were recorded at room temperature using a Nicolet FTIR Nexus with a 4 cm^{-1} resolution in the range of $4000\text{--}400 \text{ cm}^{-1}$. The test mode was set to total reflection.

Table 1 Dry weight composition of the XNBRL mixture

Raw material	XNBRL	S	ZnO	ZDC	C	casein	Peregal-O	KOH	BX
Dry weight (wt%)	100	0.5	1	1	2	0.1–0.5	0.1–0.5	0.1–0.3	0.1

X-ray diffraction (XRD) was performed on a TD3500 X-ray diffractometer (China DanDong TongDa) under the following conditions: Cu K α radiation ($\lambda = 0.15406$ nm) at a voltage of 35 kV. The scanning rate was 10°/min over a range of 10–70°. Thermogravimetric analyses (TGA) were conducted by utilizing an SDT Q600 instrument (TA, USA) from 30 to 700 °C at 20 °C/min. The tensile properties (tensile strength and elongation at break) of the film were tested using a tensile strength tester (AI-3000, Gotech Testing Machines Inc.). The hardness of the films was measured using a shore durometer (LX-A, China Jun Ping Machinery Factory).

2.5 Gamma ray attenuation measurements

Canberra's portable In Situ Object Counting System (ISOCS) passive efficiency calibration machine for low-background high-purity germanium (HPGe) gamma spectrometry was used to measure the γ -ray spectra. The probe was a coaxial germanium detector. Its sensitive area was \varnothing 80 mm \times 30 mm, and its energy resolution was 474 eV. The instrument was cooled with liquid nitrogen for more than six hours before operation. The radiation sources were ²⁴¹Am (59.5 keV) and ¹³³Ba (30.7 keV and 81.0 keV). The doses of the sources were in the millicurie range. The distance between the radiation source and the HPGe probe surface was over 25 cm, which reduced the probability of coincidence and cascading. Each sample was tested under each energy for 360 s. The peak intensity of the γ -rays was calculated as the peak area.

The γ -rays attenuation equation can be calculated using Beer and Lambert's law [21]:

$$I(d) = I_0 e^{-\mu d}, \quad (1)$$

where $I(d)$ and I_0 are the peak intensity of the γ -rays with and without the Bi₂O₃/XNBR film between the radiation source and the HPGe probe, respectively. d is the thickness of the Bi₂O₃/XNBR film. μ is the linear attenuation coefficient of the Bi₂O₃/XNBR film, which can be obtained by measuring I_0 , $I(d)$, and d .

For a given material, if μ is obtained by Eq. (1), its attenuation efficiency (AE) with an arbitrary thickness of d can be evaluated by Eq. (2) [22]:

$$AE = \frac{I_0 - I(d)}{I_0} \times 100\% = (1 - e^{-\mu d}) \times 100\%. \quad (2)$$

For a given material, if an attenuation efficiency for the actual working conditions is required, the requisite d of the material can be determined by Eq. (2).

3 Results and discussion

3.1 Dispersion state of Bi₂O₃ in the XNBR

Obtaining a uniform and stable dispersion of Bi₂O₃ in the XNBRL is a challenging because of the density inhomogeneity. Adding Bi₂O₃ powder directly into XNBRL leads to uneven dispersion, particle agglomeration, and sedimentation problems. The Bi₂O₃ powders must be well dispersed before being added into the XNBRL. The well-dispersed Bi₂O₃ was realized by milling. The granular shape of the Bi₂O₃ particles does not change after being milled. As shown in Fig. 1, after being milled for 12 h, the D₅₀ of the Bi₂O₃ particles decreased from 13.7 to 8.1 μ m, and their specific surface area increased from 0.488 to 0.763 m² g⁻¹. A larger specific surface area corresponded to a better dispersity. This revealed that milling was beneficial to the dispersal of Bi₂O₃ particles in water.

Without BX, the Bi₂O₃ powder settled within 1 h (upper left in Fig. 2a). With BX, the sedimentation of the Bi₂O₃ powder was negligible within 1 h (upper right in Fig. 2a). The dispersion state of Bi₂O₃ in the water directly influenced the dispersion state of Bi₂O₃ in the XNBRL. A well-dispersed Bi₂O₃ dispersion may not lead to a well-dispersed state of Bi₂O₃ in the XNBRL. However, an under-dispersed Bi₂O₃ dispersion led to an under-dispersed state of Bi₂O₃ in the XNBRL (lower left in Fig. 2a).

The molecular formulas of Bi₂O₃, BX, and XNBR are shown in Fig. 2b. The FTIR spectra of Bi₂O₃ and BX are shown in Fig. 2c. The broad peak at 3455 cm⁻¹ (peak 1) was attributed to the associate hydrogen bond O–H stretching. The O–H was formed by the interaction of O in the Bi₂O₃ with H in the H₂O. The peak at 400–1200 cm⁻¹ was attributed to the Bi–O deformation (Bi₂O₃) [23]. The peak at 3068 cm⁻¹ (peak 2) was attributed to the C–H stretching (naphthalene). The peak at 1680 cm⁻¹ (peak 3) was attributed to the C=C stretching (naphthalene). The peak at 1380 cm⁻¹ (peak 4) was attributed to the C–H deformation (–C₄H₉). The peak at 845 cm⁻¹ (peak 5) was attributed to C–C stretching. The peak at 650 cm⁻¹ (peak 6) was attributed to the –SO₃Na deformation. After adding 0.3% BX into Bi₂O₃, the FTIR spectra of Bi₂O₃ were not clear, as they were obscured by the FTIR spectra of BX.

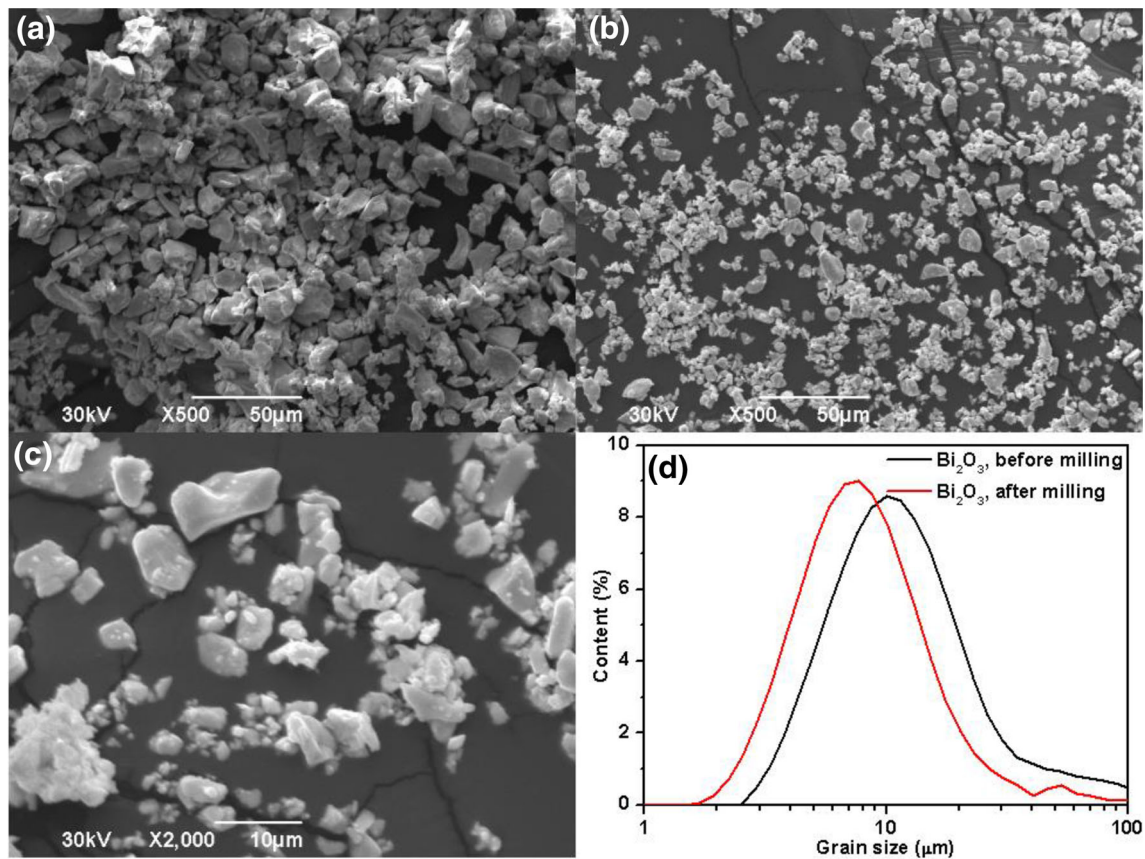


Fig. 1 (Color online) SEM images of the Bi_2O_3 particles before milling (a) and after milling for 12 h (b, c); grain size distribution of the Bi_2O_3 particles before and after milling for 12 h (d)

This suggests that the affinity interaction between BX and Bi_2O_3 was significant (Fig. 2c). The BX contains a hydrophilic ($-\text{SO}_3\text{Na}$) and a lipophilic group ($-\text{C}_{18}\text{H}_{24}$). As a commonly used surfactant, the hydrophilic property of the BX can increase the dispersal of the filler particles in water [24].

After the Bi_2O_3 dispersion and XNBRL were mixed together, casein and Pregel-O solution were added as a thickener and stabilizer, respectively, to prevent the sedimentation of the Bi_2O_3 particles in the XNBRL. According to Stokes law, the gravity settling velocity is proportional to the square of the particle radius and inversely proportional to the viscosity of the dispersal medium [25]. The viscosity of the latex was controlled by adjusting its casein and Pregel-O contents. The proper viscosity of an XNBRL mixture was 60–80 mPa s. When the Bi_2O_3 content was less than 50 wt%, the sedimentation in the Bi_2O_3 /XNBRL mixture was not obvious even after 5 days. When the Bi_2O_3 content was 50–70 wt%, sedimentation occurred over time. After stirring, the sedimentation was re-dispersed. For a Bi_2O_3 /XNBRL mixture containing more than 70 wt% Bi_2O_3 , the sedimentation problem was considerable, which needs to be solved. The preparation of a Bi_2O_3 /

XNBRL film with a higher filler content with good stability is one of the possible directions in the future.

In summary, physical and chemical methods were used to tackle the sedimentation problem of Bi_2O_3 . Physical methods were used to reduce the particle radius and to increase the latex viscosity. The chemical method consisted of adding a dispersant.

SEM images and EDS images of the 50 wt% Bi_2O_3 /XNBRL flexible films are shown in Fig. 3. There were no pores or cracks observed in the films. The EDS images of Bi, C, N, O, Zn, S, and K are presented in Fig. 3b–h, respectively. The elements Bi, C, N, O, Zn, S, and K were well distributed in the Bi_2O_3 /XNBRL flexible films, indicating that the Bi_2O_3 particles and other agents were well distributed in the XNBRL.

3.2 XRD of the Bi_2O_3 /XNBRL films

The XRD pattern of the XNBRL and Bi_2O_3 /XNBRL flexible films is shown in Fig. 4. The raw XNBRL denotes the raw material purchased without an added compounding agent. The sole peak at 19° revealed the amorphous structure of the XNBRL [26]. After vulcanization, the peak

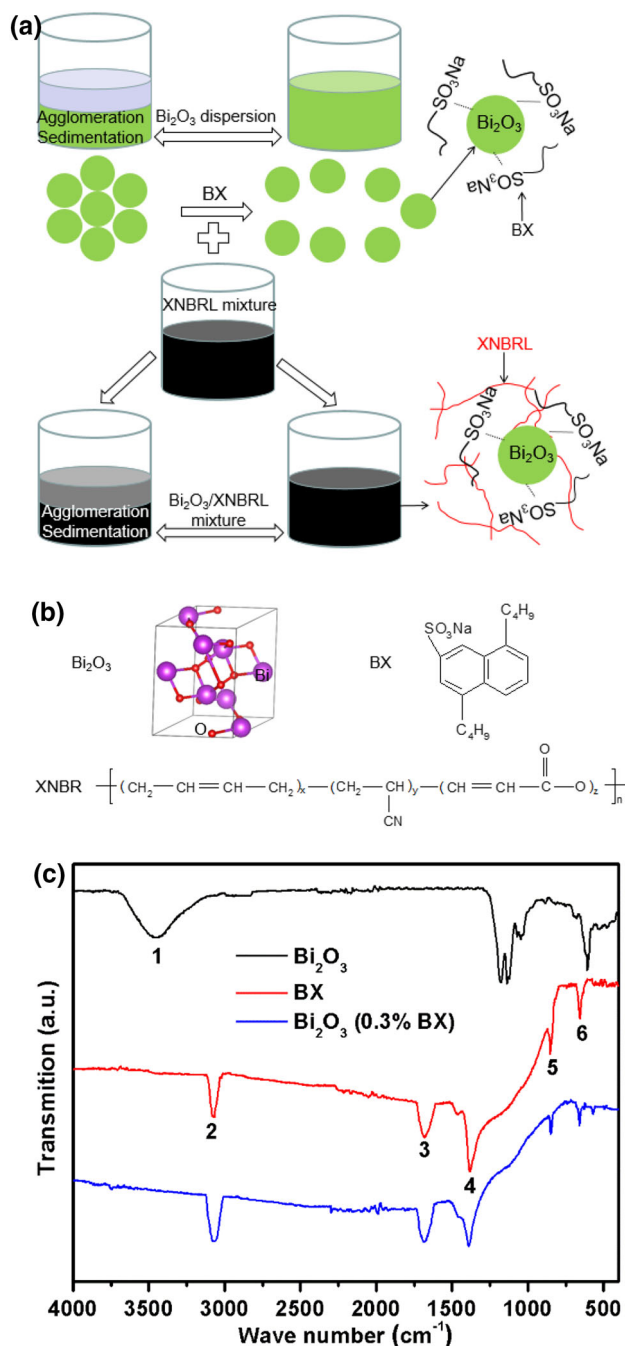


Fig. 2 (Color online) **a** Diagrammatic sketch of the dispersion state of Bi₂O₃ in the XNBR; **b** molecular formula of Bi₂O₃, BX and XNBR; **c** FTIR spectra of Bi₂O₃ and BX

amplitude weakened, and the peak position shifted to the right by 1°–20°. The three main peaks of Bi₂O₃ were observed at 27°, 33°, and 46°. The XRD pattern of Bi₂O₃ was identical to the standard card (JCPDS: 41-1449) [27, 28]. The used Bi₂O₃ was an alpha-type monoclinic system ($a = 0.585$ nm, $b = 0.817$ nm, $c = 0.751$ nm). The relative peak amplitude at 20° weakened, and the relative peak amplitudes of the three main peaks of Bi₂O₃ increased

with the increasing Bi₂O₃ content in the XNBR. After the added Bi₂O₃ exceeded 70 wt%, the XRD pattern of the Bi₂O₃/XNBR flexible films was close to that of Bi₂O₃, and the peak from XNBR was not clearly resolved.

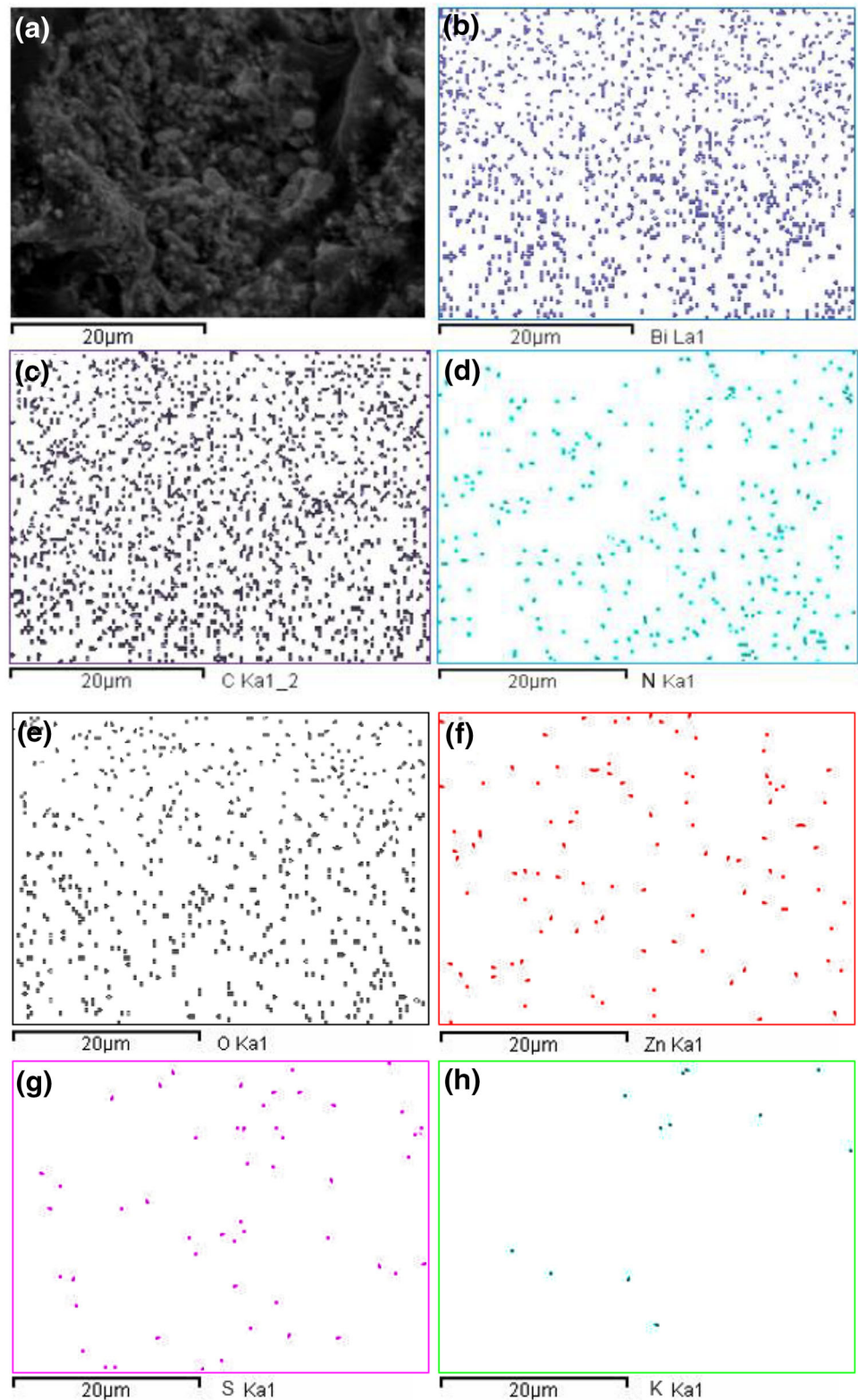
3.3 FTIR spectroscopy of the Bi₂O₃/XNBR films

The FTIR spectra of the Bi₂O₃/XNBR films are shown in Fig. 5. The characteristic IR bands of the XNBR agreed with the literature data, which is illustrated as follows [29–31]: The peak at 3457 cm⁻¹ was attributed to the O–H stretching. The peak at 2926–2920 cm⁻¹ was attributed to the CH₂ stretching (butadiene). The peak at 2851–2846 cm⁻¹ was attributed to the CH₂ stretching (acrylonitrile). The peak at 2237 cm⁻¹ was attributed to the C≡N stretching (acrylonitrile). The positions of these three peaks did not change before and after curing. The peak at 1737–1731 cm⁻¹ for XNBR was attributed to the C=O stretching (carboxyl). After vulcanization, the C=O stretching vibration peak was no longer detected, which demonstrated that the unsaturated C=O bond transformed into a saturated bond during the process. Hence, the curing reaction of the C=O bond was complete. The peak at 1698 cm⁻¹ was attributed to the C=C stretching (isoprene). This peak appeared in the raw XNBR spectrum but not in the XNBR and Bi₂O₃/XNBR spectra, which demonstrated that the C=C bond (isoprene) became a saturated bond after the vulcanization. Hence, the curing reaction of the C=C bond (isoprene) was complete. The peak at 1596 cm⁻¹ was attributed to the stretching of the zinc carboxylate salt [32]. This peak did not appear in the XNBR and Bi₂O₃/XNBR, but appeared in the raw XNBR. This result also suggested that a reaction occurred between the C=O and ZnO. The peak at 1440–1437 cm⁻¹ was attributed to C–H deformation. The peak at 1188–1183 cm⁻¹ was attributed to C–C stretching (carboxyl). The peak at 1044–1035 cm⁻¹ was attributed to C–C stretching. The peak at 968–966 cm⁻¹ was attributed to H–C=C deformation (main chain, carboxyl group). The peak at 919–909 cm⁻¹ was attributed to H–C=C deformation (side chain).

3.4 TGA of the Bi₂O₃/XNBR films

The TGA results for the XNBR and Bi₂O₃/XNBR films are shown in Fig. 6. The vertical axis is the mass loss of the sample at different temperatures. The XNBR contained 10 wt% of a non-melting substance. The sum of the non-melting substance and the mass loss was 100%. The Bi₂O₃ did not melt below 700 degrees due to its high melting point (825 °C). Suppose the mass fraction of Bi₂O₃ in the Bi₂O₃/XNBR is x , and the mass loss of the Bi₂O₃/XNBR is m_1 , then, the Bi₂O₃ content was calculated as follows:

Fig. 3 (Color online) **a** SEM images and **b–h** EDS images of 50 wt% Bi₂O₃/XNBR film



$$x + 0.1(100\% - x) = 100\% - m_l, \quad (3)$$

$$x = 100\% - m_l/0.9. \quad (4)$$

The mass loss of the nominal 30 wt% Bi₂O₃/XNBR was 63 wt%. The Bi₂O₃ content was calculated as follows: $100 - 63\% / 0.9 = 30\%$, indicating that the Bi₂O₃ content was

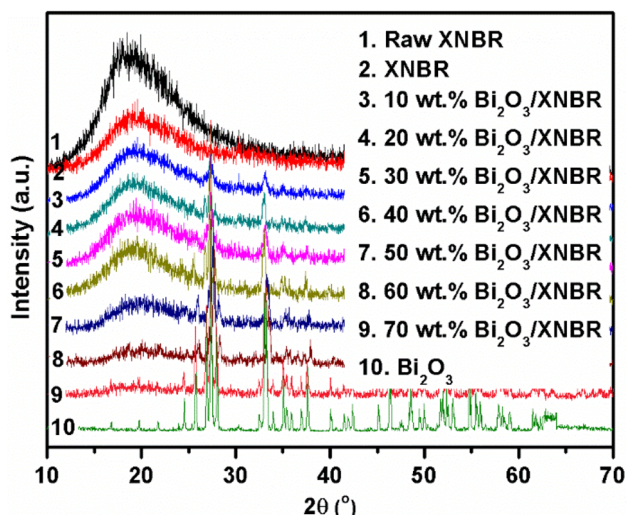


Fig. 4 (Color online) XRD pattern of the Bi₂O₃, XNBR, and Bi₂O₃/XNBR films

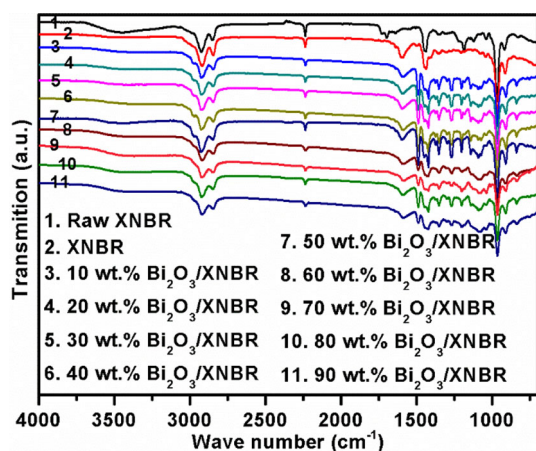


Fig. 5 (Color online) FTIR spectra of the XNBR and Bi₂O₃/XNBR films

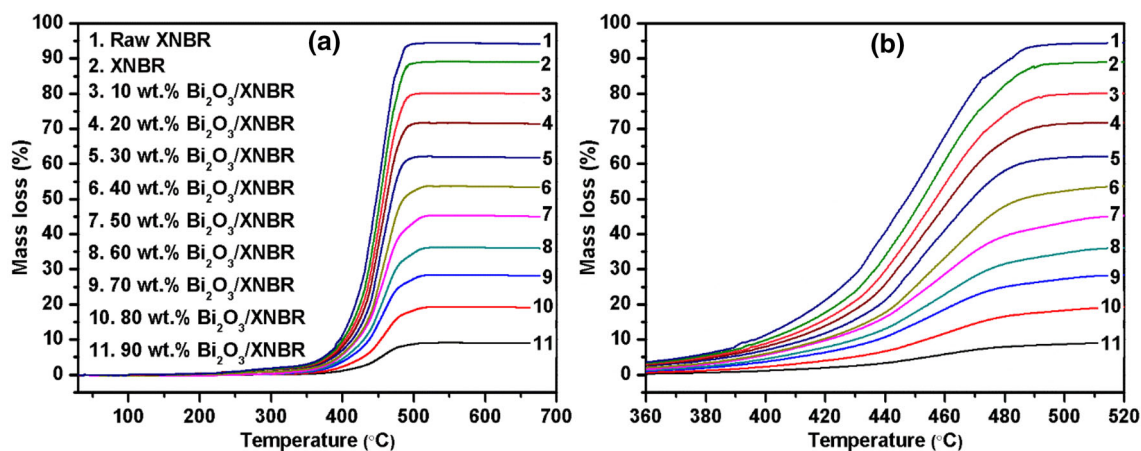


Fig. 6 (Color online) TGA of the XNBR and Bi₂O₃/XNBR films: a total, b segment

about 30 wt% and so on. The results indicate that the designed contents of Bi₂O₃ in the Bi₂O₃/XNBR films are in line with the actual contents.

The decomposition temperature obtained from TGA is a measure of thermal stability [33, 34]. The $T_{10\%}$ is the temperature at which 10% of the initial mass is lost. The decomposition temperatures of the XNBR and Bi₂O₃/XNBR films are specified in Table 2. With the increase in the Bi₂O₃ content, the decomposition temperature of the Bi₂O₃/XNBR films increased. This result indicates that Bi₂O₃ improves the thermal stability of XNBR.

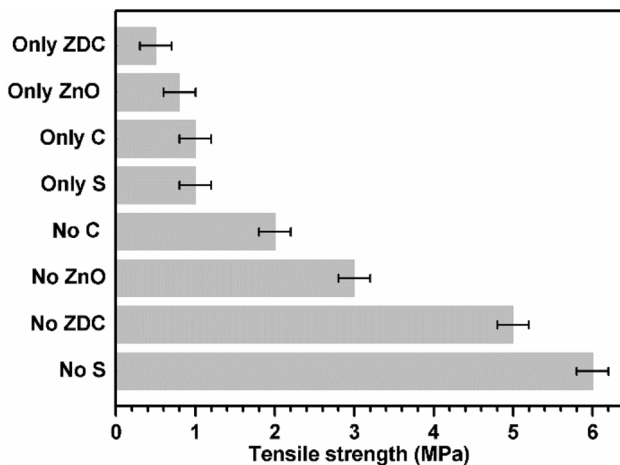
3.5 Mechanical properties of the Bi₂O₃/XNBR films

The tensile strength of the un-vulcanized XNBR was 0.3 MPa (1 MPa = 10 kgf cm⁻²), and its elongation at break was 3000%. XNBR must be vulcanized for practical applications. The compounding agent is indispensable, as illustrated in Fig. 7. The XNBR film was not strong enough without the added compounding agent. The vertical ordinate in Fig. 7 shows the use of only ZDC, ZnO, C, and S as the compounding agents and the absence of C, ZnO, ZDC, and S. The tensile strength of the vulcanized XNBR was 27 MPa with the appropriate compounding agents and vulcanization conditions (100 °C, 60 min), with an elongation at break of 1283%. These values were higher than the previously reported ones [35].

The tensile properties of the flexible films with different Bi₂O₃ contents are characterized in Fig. 8. As the Bi₂O₃ content increased, the tensile strength and elongation at break of the Bi₂O₃/XNBR films decreased. This is caused by the filler-particle concentration dependence of the composite mechanical properties [36]. When the Bi₂O₃/XNBR system contained a sufficient amount of the reinforcement agent, the additional increase in the Bi₂O₃

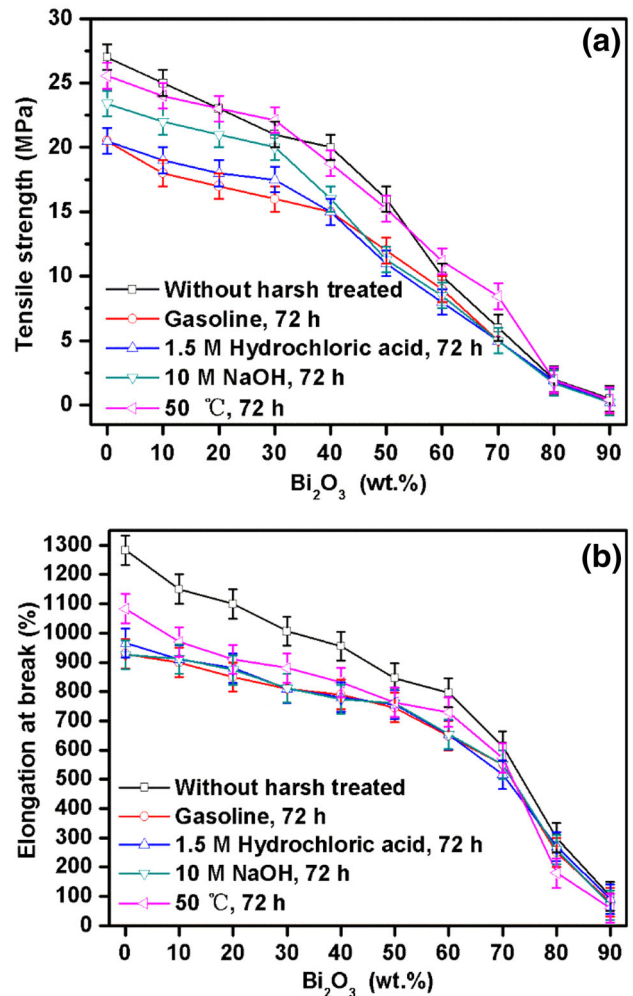
Table 2 Degradation temperatures of the XNBR and Bi₂O₃/XNBR films

Sample	Degradation temperature (°C)				
	T _{10%}	T _{20%}	T _{30%}	T _{50%}	T _{90%}
Raw XNBR	397	417	431	447	481
XNBR	401	423	436	452	512
10 wt% Bi ₂ O ₃ /XNBR	404	428	440	456	—
20 wt% Bi ₂ O ₃ /XNBR	409	432	444	461	—
30 wt% Bi ₂ O ₃ /XNBR	413	437	449	468	—
40 wt% Bi ₂ O ₃ /XNBR	419	443	456	486	—
50 wt% Bi ₂ O ₃ /XNBR	422	446	462	—	—
60 wt% Bi ₂ O ₃ /XNBR	430	454	474	—	—
70 wt% Bi ₂ O ₃ /XNBR	438	463	—	—	—
80 wt% Bi ₂ O ₃ /XNBR	453	—	—	—	—
90 wt% Bi ₂ O ₃ /XNBR	—	—	—	—	—

**Fig. 7** Tensile strength of the XNBR films without appropriate compounding agents

concentration did not help further enhancing the composite strength. When the Bi₂O₃ content was below 70 wt%, the minimum tensile strength of the Bi₂O₃/XNBR film was greater than 5 MPa, and the minimum elongation at break was above 500%, which were higher values than those reported for rubber materials used for γ -ray shielding [13]. As the Bi₂O₃ content increased, the tensile properties of the film degraded. The tensile properties of the Bi₂O₃/XNBR films containing more than 70 wt% Bi₂O₃ were not suitable for applications. The preparation of a Bi₂O₃/XNBR film with a higher filler content possessing good tensile properties is one of the research directions in the future.

As for the XNBR flexible films after harsh treatment, the minimum tensile strength was above 20 MPa, and the minimum elongation at break above 900%. After successive submersion in gasoline, 1.5 M sulfamic acid, and

**Fig. 8** (Color online) **a** Tensile strength and **b** elongation at break for Bi₂O₃/XNBR flexible films under harsh environments

10 M NaOH for 72 h at room temperature, the tensile strength and the elongation at break of the Bi₂O₃/XNBR films decreased. However, the reductions were not considerable. They were close to that of the original state without the harsh treatment. This suggested that the Bi₂O₃/XNBR films were resistant to oil, acid, and alkali. For the samples with Bi₂O₃ less than 70 wt%, after the harsh treatment, the minimum tensile strength was above 5 MPa, and the minimum elongation at break above 500%, which were suitable values for general applications. The tensile properties of the Bi₂O₃/XNBR films containing more than 70 wt% Bi₂O₃ were not suitable for applications.

The mass variation ratio of the Bi₂O₃/XNBR films under harsh environments also demonstrated their resistivity to oil, acid, and alkali. As shown in Fig. 9, after successive submersion in gasoline, 1.5 M sulfamic acid, and 10 M NaOH for 72 h at room temperature, the mass ratio of the Bi₂O₃/XNBR flexible films varied within a very small

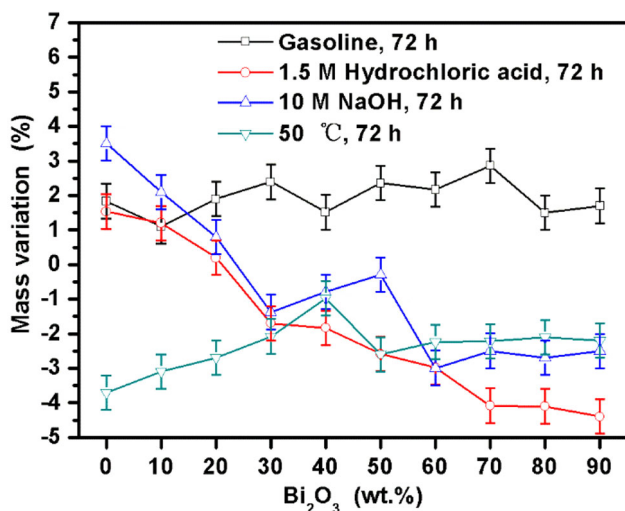


Fig. 9 (Color online) Mass variations in the Bi₂O₃/XNBR films under harsh environments

range. Figures 8 and 9 show that the Bi₂O₃/XNBR flexible films were also resistant to hot air.

As shown in Fig. 10, the raw XNBR film was very soft. After vulcanization, it was still a soft material with an enhanced shore hardness. As the Bi₂O₃ content increased, the shore hardness of the Bi₂O₃/XNBR films also increased. The films with less than 70 wt% Bi₂O₃ were still sufficiently flexible, in comparison with latex gloves, for applications. The Bi₂O₃/XNBR films containing more than 70 wt% Bi₂O₃ were too hard for applications.

A Bi₂O₃/XNBR film with an appropriate Bi₂O₃ content can be selected to satisfy the mechanical property requirements for practical applications.

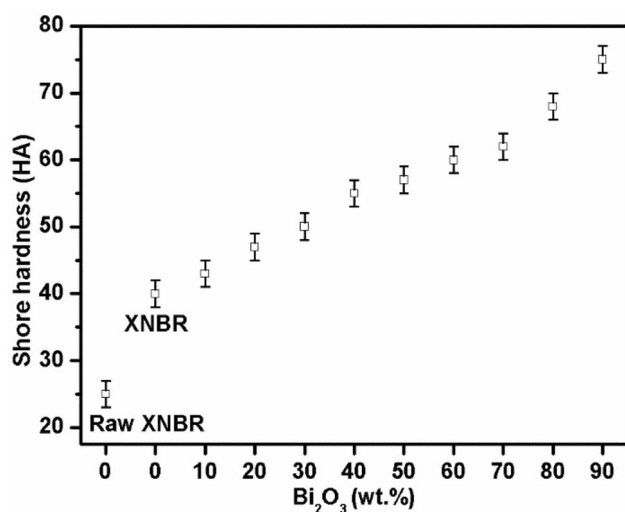


Fig. 10 Shore hardness of the Bi₂O₃/XNBR flexible films

3.6 Attenuation properties of the Bi₂O₃/XNBR films

The density of the Bi₂O₃/XNBR composite was calculated by Eq. (5):

$$\rho = \frac{m_1 + m_2}{V_1 + V_2} = \frac{\rho_2/x_2}{\rho_2x_1/\rho_1x_2 + 1}, \quad (5)$$

where the variables m , v , ρ , and x represent the mass, volume, density, and mass fraction, respectively. Subscripts 1 and 2 represent Bi₂O₃ and XNBR, respectively. Thus, $m_1/m_2 = x_1/x_2 = \rho_1v_1/\rho_2v_2$, and $x_1 + x_2 = 1$. The experimental values of ρ_1 and ρ_2 were 8.9 and 1.07 g cm⁻³, respectively, which were measured by Archimedes' principle. The density of the Bi₂O₃/XNBR flexible film is shown in Fig. 11a. The experimental and calculated values were in good agreement.

The mass attenuation coefficient of the Bi₂O₃/XNBR was calculated by Eq. (6): [37, 38]

$$\mu_m = \mu_{m,1} \cdot x_1 + \mu_{m,2} \cdot x_2 = \frac{\mu}{\rho}, \quad (6)$$

where μ_m is the mass attenuation coefficient of the Bi₂O₃/XNBR. The variables μ and ρ are the line attenuation coefficient and density of the Bi₂O₃/XNBR, respectively. The variables $\mu_{m,1}$ and $\mu_{m,2}$ are the mass attenuation coefficient of Bi₂O₃ and XNBR, respectively. The mass attenuation coefficients of Bi₂O₃ for γ -rays can be obtained through a Monte Carlo simulation or literature database research. The mass attenuation coefficient of Bi₂O₃ for 59.5 keV γ -rays was 0.42736 m² kg⁻¹ as simulated by the Monte Carlo method, which was consistent with the literature value [39]. Because XNBR is mainly composed of carbon, the mass attenuation coefficient of XNBR was approximately equal to that of carbon. According to the literature, the mass attenuation coefficient of carbon for 59.5 keV γ -rays is 0.017 m² kg⁻¹ [40].

The linear attenuation coefficient of Bi₂O₃ for low-energy γ -rays was slightly lower than that of PbO (Fig. 11a). However, Bi₂O₃ is non-toxic, which is an advantage.

The linear attenuation coefficient of the Bi₂O₃/XNBR flexible film was calculated by Eq. (7):

$$\mu = (\mu_{m,1} \cdot x_1 + \mu_{m,2} \cdot x_2) \cdot \frac{\rho_2/x_2}{\rho_2x_1/\rho_1x_2 + 1}. \quad (7)$$

The linear γ -ray attenuation coefficients of the Bi₂O₃/XNBR flexible film for energies 30.7, 59.5, and 81.0 keV are shown in Fig. 11b, c. The experimental values of μ obtained from Eq. (1) and the calculated values from Eq. (7) were in good agreement and consistent with the literature [27]. Ideally, the higher the Bi₂O₃ content, the greater the γ -ray attenuation. Since each sample was

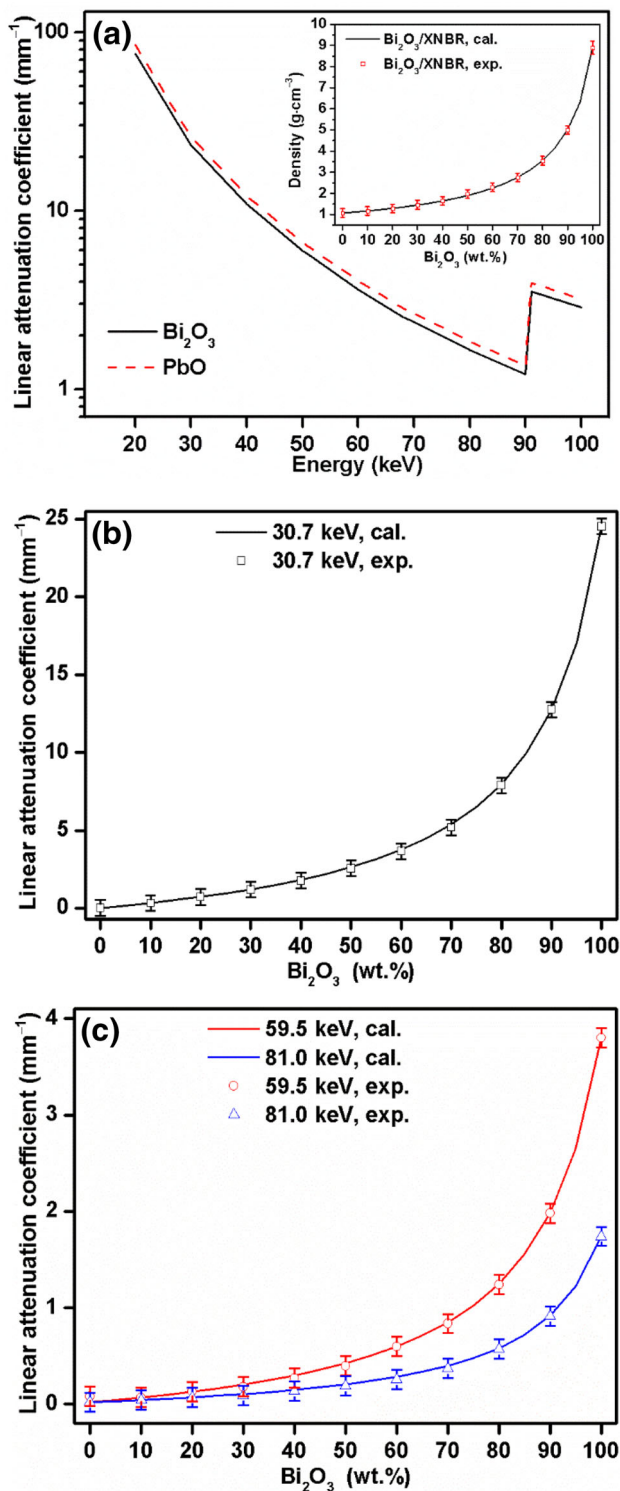


Fig. 11 (Color online) **a** Linear attenuation coefficients of Bi_2O_3 and PbO, inset image: densities of the $\text{Bi}_2\text{O}_3/\text{XNBR}$ films; **b**, **c** linear γ -ray attenuation coefficients of the $\text{Bi}_2\text{O}_3/\text{XNBR}$ films

exposed to each energy only for a short time, there no obvious change was observed through SEM after the low-energy γ -ray attenuation test.

The attenuation efficiencies of the $\text{Bi}_2\text{O}_3/\text{XNBR}$ flexible films, with different thicknesses and different Bi_2O_3 contents, for selected γ -ray energies, were calculated by Eq. (2). Figure 12 presents the γ -ray attenuation efficiencies of the $\text{Bi}_2\text{O}_3/\text{XNBR}$ flexible films for energies 30.7, 59.5, and 81.0 keV, respectively. The attenuation efficiency of the $\text{Bi}_2\text{O}_3/\text{XNBR}$ flexible films for low-energy (20–100 keV) γ -rays can be obtained using the same method. This investigation aids the engineering design. If an attenuation efficiency requirement is proposed, a suitable thickness and Bi_2O_3 content can be used to satisfy it. For a $\text{Bi}_2\text{O}_3/\text{XNBR}$ flexible film, the Bi_2O_3 content can be calculated by measuring its density and the thickness of the film, and then, its γ -ray attenuation efficiency can be assessed.

4 Conclusion

The design, development, and investigation of $\text{Bi}_2\text{O}_3/\text{XNBR}$ flexible films were successfully conducted. The important conclusions are summarized below:

The Bi_2O_3 sedimentation problem in the XNBRL was solved by reducing the Bi_2O_3 particle radius, increasing the viscosity of the latex, and adding a dispersant. The microscopy results confirmed that Bi_2O_3 was well dispersed in the XNBRL.

When the Bi_2O_3 content was below 70 wt%, the tensile strength of the $\text{Bi}_2\text{O}_3/\text{XNBR}$ film was greater than 5 MPa, and the minimum elongation at break was above 500%. The prepared $\text{Bi}_2\text{O}_3/\text{XNBR}$ flexible films prepared by dip-molding were resistant to oil, acid, alkali, and hot air. As the Bi_2O_3 content increased, the mechanical properties of the films degraded. The mechanical properties of the $\text{Bi}_2\text{O}_3/\text{XNBR}$ films containing more than 70 wt% Bi_2O_3 were not suitable for applications. The preparation of a $\text{Bi}_2\text{O}_3/\text{XNBR}$ film with a higher filler content and good mechanical properties is one of the research directions in the future.

The linear attenuation coefficients of the $\text{Bi}_2\text{O}_3/\text{XNBR}$ films experimentally obtained were in good agreement with the calculated values. The attenuation efficiencies of the $\text{Bi}_2\text{O}_3/\text{XNBR}$ films with different thicknesses and different Bi_2O_3 contents were obtained. The results demonstrated that the $\text{Bi}_2\text{O}_3/\text{XNBR}$ flexible films have a good attenuation effect for low-energy (20–100 keV) γ -rays.

This work aids the engineering and design of the films. A $\text{Bi}_2\text{O}_3/\text{XNBR}$ film with an appropriate Bi_2O_3 content can be selected to meet the requirements on mechanical properties, thickness, and attenuation efficiency in practical applications.

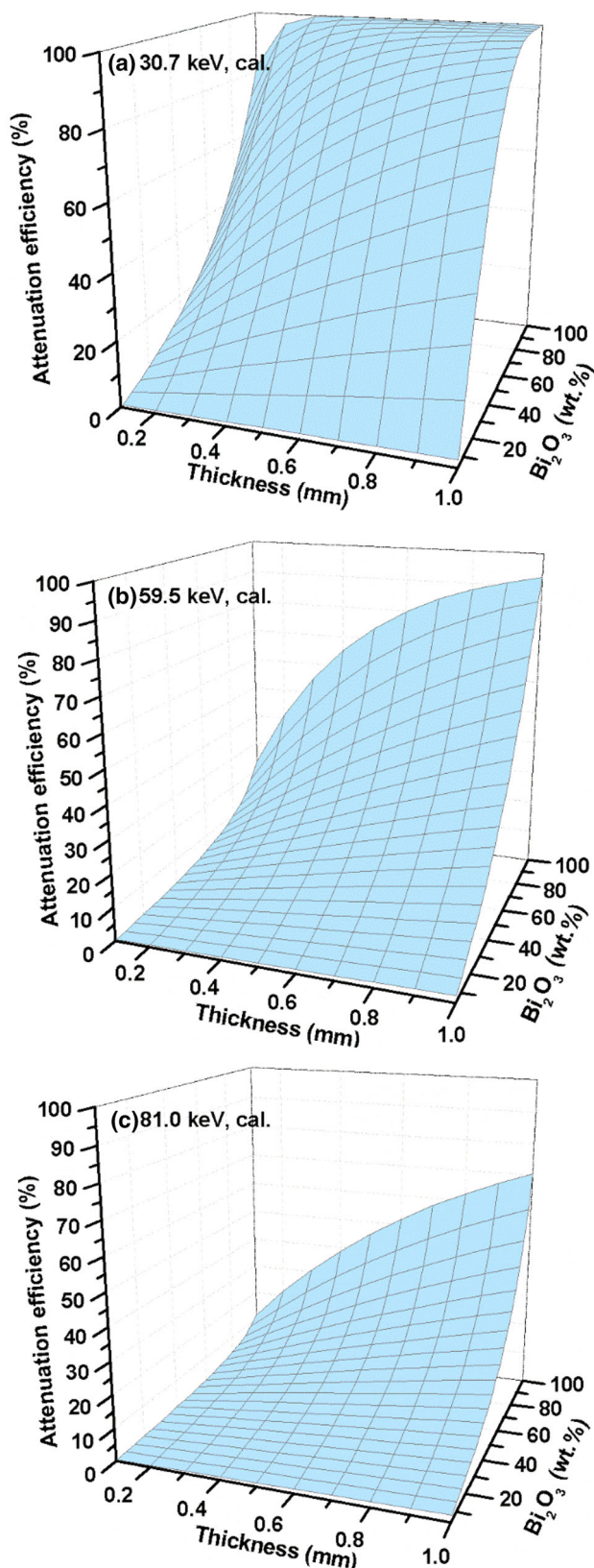


Fig. 12 Attenuation efficiencies of the Bi₂O₃/XNBR films for γ -ray energies: **a** 30.7 keV, **b** 59.5 keV, and **c** 81.0 keV

References

1. S. Fu, Y. Sun, Y. Lu, Current status of radiation therapy for prostate cancer. *Nucl. Sci. Tech.* **18**, 65–72 (2007). [https://doi.org/10.1016/S1001-8042\(07\)60021-9](https://doi.org/10.1016/S1001-8042(07)60021-9)
2. Q. Liu, B. Jiang, L.P. Jiang et al., Clinical report of three cases of acute radiation sickness from a ⁶⁰Co radiation accident in Henan province in China. *J. Radiat. Res.* **49**, 63–69 (2008). <https://doi.org/10.1269/jrr.07071>
3. S. Zhao, S. Huang, S. Liu et al., Measurements of ¹³⁴Cs and ¹³⁷Cs in urine and estimation of the internal dose of an adult exposed to the Chernobyl Accident. *Nucl. Sci. Tech.* **18**, 115–117 (2007). [https://doi.org/10.1016/S1001-8042\(07\)60030-X](https://doi.org/10.1016/S1001-8042(07)60030-X)
4. I. Akkurt, H. Akyıldırım, B. Mavi et al., Photon attenuation coefficients of concrete includes barite in different rate. *Ann. Nucl. Energy* **37**, 910–914 (2010). <https://doi.org/10.1016/j.anucene.2010.04.001>
5. M.E. Medhat, Y. Wang, Investigation on radiation shielding parameters of oxide dispersion strengthened steels used in high temperature nuclear reactor applications. *Ann. Nucl. Energy* **80**, 365–370 (2015). <https://doi.org/10.1016/j.anucene.2015.01.044>
6. M.H. Kharita, M. Takeyeddin, M. Alnassar et al., Development of special radiation shielding concretes using natural local materials and evaluation of their shielding characteristics. *Prog. Nucl. Energy* **50**, 33–36 (2008). <https://doi.org/10.1016/j.pnucene.2007.10.004>
7. N. Singh, K.J. Singh, K. Singh et al., Comparative study of lead borate and bismuth lead borate glass systems as gamma-radiation shielding materials. *Nucl. Instrum. Methods Phys. Res., Sect. B* **225**, 305–309 (2004). <https://doi.org/10.1016/j.nimb.2004.05.016>
8. J. Kim, D. Seo, B.C. Lee et al., Nano-W dispersed gamma radiation shielding materials. *Adv. Eng. Mater.* **16**, 1083–1089 (2014). <https://doi.org/10.1002/adem.201400127>
9. W. Qin, D. Peng, X. Wu, Study on the damage effects of electron and proton combined irradiation on T700/cyanate composites. *Nucl. Instrum. Methods Phys. Res., Sect. B* **312**, 126–130 (2013). <https://doi.org/10.1016/j.nimb.2013.07.017>
10. J.P. McCaffrey, H. Shen, B. Downton et al., Radiation attenuation by lead and nonlead materials used in radiation shielding garments. *Med. Phys.* **34**, 530–537 (2007). <https://doi.org/10.1118/1.2426404>
11. D.N.A. Doodoo-Amoo, S. Landsberger, J.M. MacDonald et al., Development of composite materials for non-lead gloves for use in radiological hand protection. *Health Phys.* **84**, 737–746 (2003). <https://doi.org/10.1097/00004032-200306000-00006>
12. M.E. Cournoyer, G.L. George, R.L. Dodge et al. Replacement of lead-loaded glovebox glove with attenuation medium that are not RCRA-hazardous metals. 2010, 17th Pacific Basin Nuclear Conference Cancun mexico
13. H. Chai, X.B. Tang, M.X. Ni et al., Preparation and properties of novel, flexible, lead-free X-ray-shielding materials containing tungsten and bismuth(III) oxide. *J. Appl. Polym. Sci.* **133**, 43012–43018 (2016). <https://doi.org/10.1002/app.43012>
14. M. Mirzaei Aliabadi, G. Naderi, S.J. Shahtaheri et al., Transport properties of carboxylated nitrile butadiene rubber (XNBR)-nanoclay composites; a promising material for protective gloves in occupational exposures. *J. Environ. Health Sci. Eng.* **12**, 51–58 (2014). <https://doi.org/10.1186/2052-336x-12-51>
15. M.A. Misman, A.R. Azura, Z.A.A. Hamid, The physical and degradation properties of starch-graft-acrylonitrile/carboxylated nitrile butadiene rubber latex films. *Carbohydr. Polym.* **128**, 1–10 (2015). <https://doi.org/10.1016/j.carbpol.2015.04.004>
16. K.P. Nair, A.B. Nair, R. Joseph, Carboxylated acrylo nitrile butadiene rubber latex/kaolin nanocomposites: preparation and

- properties. *Compos. Interfaces* **21**, 571–583 (2014). <https://doi.org/10.1080/15685543.2014.899198>
17. G. Marković, M.S. Marinović-Cincović, V. Jovanović et al., Gamma irradiation aging of NBR/CSM rubber nanocomposites. *Compos. B Eng.* **43**, 609–615 (2012). <https://doi.org/10.1016/j.compositesb.2011.11.056>
 18. S.E. Gwaily, M. Madani, H.H. Hassan, Lead—Natural rubber composites as gamma radiation shields. II: high concentration. *Polym. Compos.* **23**, 495–499 (2002). <https://doi.org/10.1002/pc.10450>
 19. S.A.M. Issa, A.M.A. Mostafa, Effect of Bi₂O₃ in borate-tellurite-silicate glass system for development of gamma-rays shielding materials. *J. Alloys Compd.* **695**, 302–310 (2017). <https://doi.org/10.1016/j.jallcom.2016.10.207>
 20. W. Hao, Y. Gao, X. Jing et al., Visible light photocatalytic properties of metastable γ -Bi₂O₃ with different morphologies. *J. Mater. Sci. Technol.* **30**, 192–196 (2014). <https://doi.org/10.1016/j.jmst.2013.09.023>
 21. B.A. Benetskii, M.V. Plotnikova, Gamma-radiation accumulation factors for composite materials and radiation shields. *Bull. Lebedev. Phys. Inst.* **39**, 113–117 (2012). <https://doi.org/10.3103/S1068335612040045>
 22. V.P. Singh, S.P. Shirmardi, M.E. Medhat et al., Determination of mass attenuation coefficient for some polymers using Monte Carlo simulation. *Vacuum* **119**, 284–288 (2015). <https://doi.org/10.1016/j.vacuum.2015.06.006>
 23. S. Hariharan, R. Udayabhaskar, T.R. Ravindran et al., Surfactant assisted control on optical, fluorescence and phonon lifetime in α -Bi₂O₃ microrods. *Spectrochim. Acta, Part A* **163**, 13–19 (2016). <https://doi.org/10.1016/j.saa.2016.02.045>
 24. S. Chakraborty, I. Sarkar, D.K. Behera et al., Experimental investigation on the effect of dispersant addition on thermal and rheological characteristics of TiO₂ nanofluid. *Powder Technol.* **307**, 10–24 (2017). <https://doi.org/10.1016/j.powtec.2016.11.016>
 25. P.C. Hiemenz, R. Rajagopalan, *Principles of Colloid and Surface Chemistry* (Marcel Dekker, New York, 1997)
 26. Z.N. Ain, A.R. Azura, Effect of different types of filler and filler loadings on the properties of carboxylated acrylonitrile–butadiene rubber latex films. *J. Appl. Polym. Sci.* **119**, 2815–2823 (2011). <https://doi.org/10.1002/app.32984>
 27. M.R. Ambika, N. Nagaiah, V. Harish et al., Preparation and characterisation of Isophthalic-Bi₂O₃ polymer composite gamma radiation shields. *Radiat. Phys. Chem.* **130**, 351–358 (2017). <https://doi.org/10.1016/j.radphyschem.2016.09.022>
 28. R. Sharma, M. Khanuja, S.N. Sharma et al., Reduced band gap & charge recombination rate in Se doped α -Bi₂O₃ leads to enhanced photoelectrochemical and photocatalytic performance: theoretical & experimental insight. *Int. J. Hydrog. Energy* **42**, 20638–20648 (2017). <https://doi.org/10.1016/j.ijhydene.2017.07.011>
 29. L. Wang, W. Wang, Y. Fu et al., Enhanced electrical and mechanical properties of rubber/graphene film through layer-by-layer electrostatic assembly. *Compos. Part B Eng.* **90**, 457–464 (2016). <https://doi.org/10.1016/j.compositesb.2015.12.048>
 30. X. He, T. Li, Z. Shi et al., Thermal-oxidative aging behavior of nitrile-butadiene rubber/functional LDHs composites. *Polym. Degrad. Stab.* **133**, 219–226 (2016). <https://doi.org/10.1016/j.polymdegradstab.2016.08.018>
 31. A. Laskowska, M. Zaborski, G. Boiteux et al., Effects of unmodified layered double hydroxides MgAl-LDHs with various structures on the properties of filled carboxylated acrylonitrile–butadiene rubber XNBR. *Eur. Polym. J.* **60**, 172–185 (2014). <https://doi.org/10.1016/j.eurpolymj.2014.09.013>
 32. R.L. Sala, T.M. Arantes, E. Longo et al., Evaluation of modified silica nanoparticles in carboxylated nitrile rubber nanocomposites. *Colloids Surf. A* **462**, 45–51 (2014). <https://doi.org/10.1016/j.colsurfa.2014.08.012>
 33. Y. Han, L.X. Mao, H.W. Meng et al., Novel self-crosslinking film from hydrogenated carboxylated nitrile rubber latex. *J. Appl. Polym. Sci.* **131**, 39865–39871 (2014). <https://doi.org/10.1002/app.39865>
 34. G. Janowska, A. Kucharska-Jastrzabek, A. Kasiczak et al., Thermal properties and combustibility of cross-linked XNBR/CSM blends. *J. Therm. Anal. Calorim.* **104**, 1107–1115 (2011). <https://doi.org/10.1007/s10973-011-1328-9>
 35. T. Biswas, D.K. Basu, Cure synergism in XNBR vulcanization in presence of thiophosphoryl disulfides and amine disulfide/thiazole accelerators. *J. Appl. Polym. Sci.* **60**, 1349–1359 (1996). [https://doi.org/10.1002/\(sici\)1097-4628\(19960531\)60:9<1349::aid-app10>3.0.co;2-y](https://doi.org/10.1002/(sici)1097-4628(19960531)60:9<1349::aid-app10>3.0.co;2-y)
 36. W. Qin, D. Peng, X. Wu et al., Study on the resistance performance of TiO₂/cyanate ester nano-composites exposed to electron radiation. *Nucl. Instrum. Methods Phys. Res., Sect. B* **325**, 115–119 (2014). <https://doi.org/10.1016/j.nimb.2014.01.022>
 37. I. Akkurt, A.M. El-Khayatt, The effect of barite proportion on neutron and gamma-ray shielding. *Ann. Nucl. Energy* **51**, 5–9 (2013). <https://doi.org/10.1016/j.anucene.2012.08.026>
 38. S.A.M. Issa, Effective atomic number and mass attenuation coefficient of PbO–BaO–B₂O₃ glass system. *Radiat. Phys. Chem.* **120**, 33–37 (2016). <https://doi.org/10.1016/j.radphyschem.2015.11.025>
 39. K. Kirdsiri, J. Kaewkhao, N. Chanthima et al., Comparative study of silicate glasses containing Bi₂O₃, PbO and BaO: radiation shielding and optical properties. *Ann. Nucl. Energy* **38**, 1438–1441 (2011). <https://doi.org/10.1016/j.anucene.2011.01.031>
 40. S.M. Vahabi, M. Bahreinipour, M.S. Zafarghandi, Determining the mass attenuation coefficients for some polymers using MCNP code: a comparison study. *Vacuum* **136**, 73–76 (2017). <https://doi.org/10.1016/j.vacuum.2016.11.011>